Check for updates

Catechol–TiO$_2$ hybrids for photocatalytic H$_2$ production and photocathode assembly†‡

Katherine L. Orchard, [ID] [ab] Daisuke Hojo, [b] Katarzyna P. Sokol, [ID] [a] Meng-Ju Chan, [ID] [b] Naoki Asao, [ID] §[b] Tadafumi Adschiri*[b] and Erwin Reisner [ID] *[a]

Visible-light driven H$_2$ evolution in water is achieved using catechol-photosensitised TiO$_2$ nanoparticles with a molecular nickel catalyst. Layer-by-layer immobilisation of catechol–TiO$_2$ onto tin-doped indium oxide electrodes generates photocathodic currents in the presence of an electron acceptor. This approach represents a new strategy for controlling photocurrent direction in dye-sensitised photoelectrochemical applications.

Immobilising molecular dyes onto wide band-gap metal oxide semiconductors is a well-established strategy for preparing tuneable, visible-light responsive materials from relatively inexpensive components. This approach was pioneered for solar energy conversion in dye-sensitised solar cells (DSCs)[1] and is an emerging field in the area of solar fuels synthesis.[2] In the majority of dye-sensitised systems, photoexcitation occurs in the dye (HOMO–LUMO transition) followed by fast charge injection into the semiconductor (Type I sensitisation, Fig. 1a). This approach has been effective in H$_2$ production using dye-sensitised photocatalysis (DSP)[2a] and in forming photoanodes for dye-sensitised photoelectrochemical cells (DSPEC);[2b,c] however, the translation of DSP systems to photocathodes is more challenging, often relying on low-performance p-type semiconductors (such as NiO)[3] or molecular engineering[4] to control the direction of electron transfer.

Charge-transfer sensitisation, in which photoexcitation occurs directly from a surface-adsorbed molecule to the semiconductor conduction band (Type II, Fig. 1a), has recently been explored as a
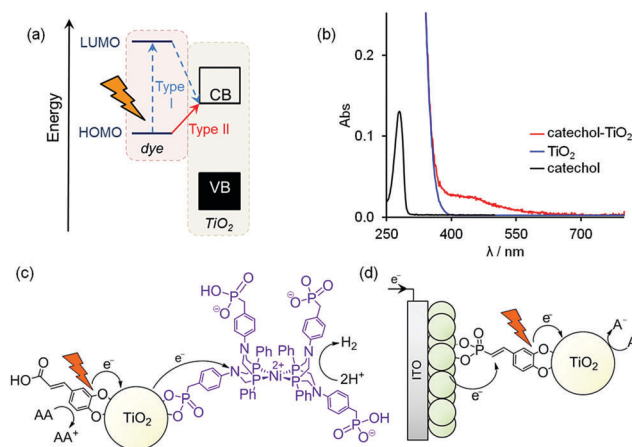

Fig. 1 (a) Energy transfer in Type I (two-step) and Type II (one-step) dye-sensitised TiO$_2$ systems; (b) diffuse reflectance absorption spectrum of catechol-modified TiO$_2$ compared to bare TiO$_2$ and the transmission spectrum of catechol in water (catechol shown is DHCA); (c) solar H$_2$ production in DSP system (AA = ascorbic acid); (d) layer-by-layer photocathode incorporating catechol–TiO$_2$ (A = acceptor; catechol shown is DHSP).

low-cost alternative in DSCs[5] and solar fuel production.[6] Type II sensitisation is known to occur in TiO$_2$ functionalised with phenol and enediol groups, such as catechols.[5d] These groups bind to Ti^{4+} ions on the surface of TiO$_2$, forming complexes that absorb visible light due to ligand-to-metal charge-transfer (Fig. 1b).[7] This one-step transfer from dye to TiO$_2$ results in very fast electron injection (on the order of fs),[5b] and, importantly, by avoiding excitation into the dye LUMO the charge-transfer is inherently directional (Fig. 1a and Fig. S1, ESI‡). Type II sensitisation also occurs between carbon nitride and TiO$_2$, and has been used to enhance solar light-driven H$_2$ evolution with hydrogenase,[8] and to form photoanodes for photoelectrochemical water oxidation.[9]

Catechol-containing dyes based on alizarin red have been studied for DSP and for photocurrent switching applications;[10] however, these dyes are also Type I sensitisers.[5d] To our knowledge, the only example of purely Type II visible-light driven H$_2$ evolution uses phenolic resin-sensitised TiO$_2$ nanoparticles,

a Department of Chemistry, University of Cambridge, Lensfield Road, Cambridge, CB2 1EW, UK. E-mail: reisner@ch.cam.ac.uk; Web: http://www.reisner.ch.cam.ac.uk
b WPI Advanced Institute for Materials Research (AIMR), Tohoku University, 2-1-1 Katahira Aoba-ku Sendai, Miyagi, 980-8577, Japan. E-mail: ajiri@tagen.tohoku.ac.jp

with Pt as the H_2 evolution catalyst (HEC) in the presence of a sacrificial electron donor (SED).[6b,c]

Replacing noble metals with inexpensive catalysts and moving towards SED-free systems are both important goals in achieving sustainable fuel synthesis. Here we take steps towards addressing these challenges by developing a new route for assembling noble metal-free photocathodes. First, we demonstrate that Pt can be replaced by a 3d transition metal catalyst to form an active Type II DSP system (Fig. 1c). We then develop a SED-free photoelectrochemical system, using the directionality of the charge-transfer complex to form photocathodes on a conductive electrode support (Fig. 1d).

For the DSP system, a range of charge-transfer dye-sensitised TiO_2 powders were prepared by mixing simple catechol derivatives (Fig. 2a) with commercial P25 TiO_2 nanoparticles (average crystallite diameter 21 nm, 8:2 mixture of anatase:rutile). The resulting coloured powders exhibited broad light absorption over the visible range (Fig. S2, ESI‡). The dye loadings ranged from 75–172 nmol (mg TiO_2)$^{-1}$ (Table S1, ESI‡). These loadings correspond to an estimated footprint of 0.5–1.1 nm^2 molecule^{-1}, consistent with reported ranges for sub-monolayer to monolayer coverage of catechols on TiO_2.[11]

Photocatalysis solutions were prepared by suspending the dye-P25 powders (2.5 mg) in aqueous SED solution (ascorbic acid, AA, 0.1 M, 2.25 mL). We selected the HEC [Ni(P$^{Ph}_2$N$^{C_6H_4CH_2P(O)(OH)_2}_2$)$_2$]Br$_2$, NiP (Fig. 1c), as it has previously been shown to be highly active in aqueous DSP[12] and DSPEC.[3a,4b] NiP (50 nmol) was added to the dye-P25 suspension as a solution in methanol (1 mM) before the photoreactors were purged with N_2 and irradiated with simulated solar light ($\lambda > 420$ nm, AM 1.5 G, 100 mW cm^{-2}). The formation of the hybrid DSP system (Fig. 1c) is supported by FTIR and UV-vis spectroscopy (Fig. S3, ESI‡), with an estimated NiP loading of 38 nmol mg^{-1} for caffeic acid (CA)-P25 (calculated using the difference in absorption at 450 nm of a NiP solution before and after exposure to TiO_2). No H_2 was detected in control experiments without AA, TiO_2 or NiP, or with NiCl$_2$ in place of NiP.

AA can also sensitise TiO_2 through charge-transfer interactions, resulting in small amounts of H_2 evolution in the absence of additional catechol during visible light irradiation (Fig. 2b, "none"); however, all ex situ functionalised powders enhanced the activity compared to bare P25 (Fig. 2b and Fig. S4a, ESI‡). The highest activity was obtained with CA (Fig. 2), with an activity with respect to the powder of 273 ± 29 μmol H_2 g^{-1} after 4 h. The activity per hour of 73 ± 3 μmol H_2 (g TiO_2)$^{-1}$ h^{-1} was maintained over the first 4 h, equivalent to a turnover frequency (TOF) per Ni catalyst of 3.6 ± 0.2 μmol H_2 (μmol NiP)$^{-1}$ h^{-1} and TOF per catechol of 0.6 ± 0.2 μmol H_2 (μmol CA)$^{-1}$ h^{-1}. This result is comparable to that reported for the phenolic resin system with Pt (105 μmol g^{-1} h^{-1}).[6b] The TOF$_{Ni}$ is an order of magnitude lower than previously reported for the equivalent system with a Ru tris(bipyridine) dye, RuP,[12] but RuP can directly reduce NiP in solution, whereas the catechol derivatives cannot. The lower extinction coefficient and faster recombination rate of the charge-transfer band relative to that of metal-based dyes (ps[13] vs. ns–μs[2a]) are also expected to contribute to the difference in activity.

The high activity of CA relative to the unconjugated analogue 3,4-dihydroxyhydrocinnamic acid (DHCA) is consistent with the red-shift in the absorption spectrum and increase in both the catechol binding constant and the electron injection efficiency associated with greater conjugation.[5b] The activity per dye molecule also reflects this trend for 2-(3,4-dihydroxybenzene)thiophene (DHBT; Fig. S4b, ESI‡); however, the lower loading of DHBT on TiO_2 compared to CA (Table S1, ESI‡) resulted in a lower activity per gram (Fig. 2b). Ring conjugation (2,3-naphthalenediol, ND) did not enhance activity (Fig. 2b and Fig. S4b, ESI‡), which is likely due to the comparatively low visible light absorption of ND-P25 (Fig. S1, ESI‡).

The turnover number per Ni (TON$_{Ni}$) increased with decreasing NiP loading (Fig. S5a, ESI‡) and increasing CA-P25 powder loading (Fig. S6a, ESI‡). However, the corresponding activity per gram decreased with decreasing NiP loading (Fig. S5b, ESI‡) and reached a maximum at a CA-P25 loading of 1.25 mg (Fig. S6b, ESI‡). Since increasing the powder loading increases both the dye loading and the particle:Ni ratio, it can be inferred that the H_2 production rate is limited by the generation and supply of electrons to NiP. This conclusion is supported by the decrease in activity of the system on decreasing the light intensity (Fig. S7, ESI‡). The external quantum efficiency (EQE) of the most active system (5 mg CA-P25, 50 nmol NiP) was measured to be 0.09 ± 0.01%.

Since light absorption is related to the number of catechol–TiO_2 surface interactions, light absorption per g can be enhanced by using smaller nanoparticles to increase the surface area. We synthesised TiO_2 nanoparticles by a previously reported method (pure anatase, average diameter ~7 nm, AN7–TiO_2, see Fig. S8, ESI‡ for TEM)[14] and tested both these and commercial pure anatase nanoparticles (10 nm, AN10–TiO_2, Fig. S7, ESI‡) under the standard DSP conditions (CA–TiO_2, 2.5 mg, 50 nmol NiP).

Fig. 2 (a) Chemical structures of charge-transfer dyes used in this study (catechol = 1,2-dihydroxybenzene, DHBA = 3,4-dihydroxybenzoic acid, DHCA = 3,4-dihydroxyhydrocinnamic acid, CA = caffeic acid, DHBT = 2-(3,4-dihydroxybenzene)thiophene, ND = 2,3-naphthalenediol, AA = ascorbic acid); (b) comparison of visible-light driven H_2 evolution with charge-transfer dye-functionalised P25 TiO_2 powders in the presence of a molecular Ni catalyst, NiP (0.1 M AA, pH 4.5, 2.5 mg powder, 50 nmol NiP, 2.25 mL, $\lambda > 420$ nm, AM 1.5 G, 100 mW cm^{-2}, 25 °C).

However, despite the increase in catechol loading (505 nmol $(mg\ TiO_2)^{-1}$; Table S1, ESI‡) and light absorption (Fig. S9, ESI‡) compared to P25, these particles displayed less photocatalytic activity (Fig. S10, ESI‡). The lower performance was not found to be due to a difference in binding of **NiP** to the particles (48 and 51 nmol mg^{-1} for AN10–TiO_2 and AN7–TiO_2, respectively). However, it is likely that the smaller, pure anatase particles suffer from less efficient charge separation compared to the larger, mixed-phase (anatase/rutile) P25.[15] Pure rutile phase TiO_2 nanoparticles (R–TiO_2, 10–30 nm) displayed lower activity than P25, AN10, and AN7–TiO_2 (4.9 ± 0.3 after 3 h, Table S2 and Fig. S10, ESI‡).

Having established that catechol–TiO_2 hybrids are effective light absorbers for (UV-filtered) solar H_2 evolution with **NiP**, we sought to transfer the DSP system onto photoelectrodes. We designed a layer-by-layer route to immobilise the TiO_2 nanoparticles onto a degenerately doped n-type metal oxide support (indium tin oxide, ITO) in a directed, sequential fashion (Fig. 1d). In order to maximise the deposition of the TiO_2 nanoparticles in our system, we used hierarchical inverse opal mesoporous ITO electrodes (IO–ITO; Fig. S11a, ESI‡). IO–ITO is an effective support for nanoscale adsorbates such as enzymes (e.g. Photosystem II, $10.5 \times 20.5 \times 11.0\ nm^3$), owing to their open, macroporous structure (750 nm pores with 150 nm interconnecting chambers) and high surface area mesoporous scaffold (formed from <50 nm ITO nanoparticles).[16] Mesoporous ITO (mesoITO) electrodes (1 µm thickness, Fig. S11b, ESI‡) were also prepared for comparison.[17]

By studying the attachment of DHCA to IO–ITO in the presence or absence of one equivalent of propylphosphonic acid by UV-vis spectroscopy, we found that ITO binds preferentially to phosphonate groups over catechol groups (83% of DHCA is displaced; Fig. S12a, ESI‡). We therefore synthesised (E)-(3,4-dihydroxystyryl)phosphonic acid (DHSP; see Fig. 1d and ESI‡ for synthetic details) as a bifunctional, phosphonated catechol that is expected to bind to ITO in the correct orientation for subsequent formation of the charge-transfer interaction with TiO_2. In contrast to ITO, TiO_2 has an approximately equal binding affinity for catechol and phosphonic acid groups (45% of DHCA was displaced in the presence of propylphosphonic acid; Fig. S12b, ESI‡). Therefore, formation of the charge-transfer complex was only effective if DHSP was anchored to ITO before adding TiO_2; ex situ-prepared DHSP-sensitised P25 powders did not absorb appreciably in the visible-light region.

DHSP was anchored onto ITO by incubating the electrodes in an aqueous stock solution (1 mM, 2–8 °C, 16 h). Cyclic voltammetry (CV) of DHSP-functionalised flat ITO shows a quasi-reversible wave ($E_{1/2} = 0.84$ V vs. RHE), which can be assigned to the catechol/semiquinone redox couple (Fig. S13, ESI‡). By monitoring the change in absorbance of a stock solution of DHSP (1 mM) at 280 nm after incubation with IO–ITO electrodes, the loading of DHSP was estimated to be 64 ± 11 nmol cm^{-2}, which matches the loading estimated from the charge passed during CV (55.5 nmol cm^{-2}, see ESI‡).

The final charge-transfer complexes were formed by depositing TiO_2 nanoparticles onto the DHSP-functionalised IO–ITO. In

contrast to the photocatalysis results, the electrodes with the highest photocurrent in the presence of an acceptor (O_2) were those prepared with AN7–TiO_2 nanoparticles (Fig. S14, ESI‡). The nanoparticles were deposited by immersion of the IO–ITO|DHSP electrodes in a stock solution of oleic acid-capped AN7–TiO_2,[18] followed by treatment with NEt_3 (10 vol% in ethanol) to remove surface oleic acid, as confirmed by FTIR spectroscopy (Fig. S15, ESI‡). The formation of the charge-transfer complex was evidenced by a change in colour of the electrodes from pale yellow/green to peach (Fig. S16, ESI‡). The loading of TiO_2 was measured to be 212.4 µg cm^{-2} for 12 µm thick IO–ITO (Ti content; Inductively Coupled Plasma-Optical Emission Spectroscopy, ICP-OES), which corresponds to approximately 83 nmol of nanoparticles per cm^2.

Scanning electron microscopy (SEM) of AN7–TiO_2 on DHSP-functionalised flat ITO showed that an even monolayer of particles is formed (Fig. S17, ESI‡), and energy-dispersive X-ray spectroscopy (EDX) of the fully assembled IO–ITO|DHSP|AN7–TiO_2 electrodes showed that the particles are evenly distributed throughout the IO–ITO structure (Ti content of 11.8, 11.4, and 10.7 at% for the top, middle, and bottom part of the IO–ITO structure respectively; Fig. S18a, ESI‡). In contrast, EDX analysis of equivalent electrodes prepared with P25 TiO_2 showed that these nanoparticles do not penetrate beyond the surface (10–12 at% Ti detected only on the top surface and none at lower layers; Fig. S18b, ESI‡). The difference in particle distribution, and subsequent performance, is attributed to the better size match of the macro- and mesopores of the IO–ITO structure to the small, well-dispersed AN7–TiO_2 compared to the larger, aggregated P25 particles (close to micron-sized aggregates of 20 nm particles; see Fig. S8, ESI‡ for TEM). AN10–TiO_2 nanoparticles also form aggregates (Fig. S8, ESI‡), resulting in low performance (Fig. S14, ESI‡).

In the presence of the electron acceptor O_2, cathodic photocurrents were obtained under visible light irradiation ($\lambda > 400$ nm, 100 mW cm^{-2}) with IO–ITO|DHSP|AN7–TiO_2 electrodes below the redox potential of DHSP ($E_{applied} = 0.3$ V vs. RHE, Fig. 3a). Initial current spikes were observed in the photocurrent curves of these electrodes (Fig. 3a), which likely occur due to rapid polarisation and charge accumulation at the electrode.[19] A switch to anodic photocurrent was observed at potentials where DHSP is oxidised ($E_{applied} > \sim 0.7$ V vs. RHE, Fig. S19, ESI‡). The photocurrent is attributed to the formation of the charge-transfer complex since little photocurrent is obtained in the absence of the catechol and/or TiO_2 (Fig. 3a). The magnitude of the photocurrent scales with the thickness of the ITO scaffold, reflecting the increase in loading of the dye–TiO_2 complex with increasing ITO surface area (Fig. 3b). The photocathodic currents obtained with 12 µm thick IO–ITO (70 µA cm^{-2}) are comparable to those obtained with Ru-based Type I dyes in the presence of an acceptor,[20] demonstrating the promise of employing metal-free Type II dyes.

In the absence of O_2 (N_2 purged solution), small cathodic currents were maintained for the bare IO–ITO|DHSP|AN7–TiO_2 electrodes (Fig. S20, ESI‡). Although **NiP** could be immobilised onto the electrodes (maximum loading of 29 ± 3 nmol per cm^2; UV-vis spectroscopy), photo-driven H_2 evolution was not achieved

Fig. 3 (a) Chronoamperograms under chopped irradiation of (i) IO−ITO|DHSP, (ii) IO−ITO, (iii) IO−ITO|AN7−TiO₂ and (iv) IO−ITO|DHSP|AN7−TiO₂ electrodes. (b) Effect of ITO morphology and thickness on visible-light photocurrent of ITO|DHSP|AN7−TiO₂ electrodes. Due to the hierarchical structure consisting of macro- and mesopores, the effective surface area of IO-2 μm ITO is lower than 1 μm mesoITO. Conditions: Na_2SO_4 (0.1 M), pH 4.5, 0.3 V vs. RHE, 100 mW cm⁻², λ > 400 nm, room temperature, under air.

with these electrodes. It is possible that the phosphonate groups in **NiP** may displace either some or all of the DHSP groups from the surface of TiO_2. **NiP** can also bind directly to ITO, by-passing the dye–TiO_2 construct. Therefore, although the layer-by-layer design successfully generates a directional, dye-sensitised electrode, further catalyst design is required in order to fully translate the DSP system to DSPEC.

In conclusion, we have demonstrated that catechol–TiO_2 complexes are effective photosensitisers for driving sacrificial H_2 evolution with an earth-abundant molecular catalyst, forming a fully noble metal-free Type II DSP system. Using a layer-by-layer method, we have transferred the dye-sensitised TiO_2 to an electrode to form a Type II photocathode. The excellent size match between the hierarchical IO–ITO support and the TiO_2 nanoparticles is critical for high dye–TiO_2 loading. The obtained photocurrents with a sacrificial electron acceptor are comparable to those obtained with Type I dyes, indicating that this is a promising means to control photocurrent direction and allow the use of n-type metal oxide supports (such as ITO) in DSPEC applications. This work represents an important first step in translating functional DSP systems to DSPEC; however, challenges in coupling these electrodes to a H_2 evolution catalyst will need to be overcome in order to apply them for sustainable solar fuels synthesis.

Conflicts of interest

There are no conflicts to declare.

Notes and references

1 A. Hagfeldt, G. Boschloo, L. Sun, L. Kloo and H. Pettersson, Chem. Rev., 2010, **110**, 6595–6663.
2 (a) J. Willkomm, K. L. Orchard, A. Reynal, E. Pastor, J. R. Durrant and E. Reisner, Chem. Soc. Rev., 2016, **45**, 9–23; (b) J. R. Swierk and T. E. Mallouk, Chem. Soc. Rev., 2013, **42**, 2357–2387; (c) L. Alibabaei, H. Luo, R. L. House, P. G. Hoertz, R. Lopez and T. J. Meyer, J. Mater. Chem. A, 2013, **1**, 4133–4145.
3 (a) M. A. Gross, C. E. Creissen, K. L. Orchard and E. Reisner, Chem. Sci., 2016, **7**, 5537–5546; (b) L. J. Antila, P. Ghamgosar, S. Maji, H. Tian, S. Ott and L. Hammarström, ACS Energy Lett., 2016, **1**, 1106–1111; (c) L. Li, L. Duan, F. Wen, C. Li, M. Wang, A. Hagfeldt and L. Sun, Chem. Commun., 2012, **48**, 988–990; (d) F. Li, K. Fan, B. Xu, E. Gabrielsson, Q. Daniel, L. Li and L. Sun, J. Am. Chem. Soc., 2015, **137**, 9153–9159; (e) Z. Ji, M. He, Z. Huang, U. Ozkan and Y. Wu, J. Am. Chem. Soc., 2013, **135**, 11696–11699.
4 (a) Z. Huang, M. He, M. Yu, K. Click, D. Beauchamp and Y. Wu, Angew. Chem., Int. Ed., 2015, **54**, 6857–6861; (b) B. Shan, A. K. Das, S. Marquard, B. H. Farnum, D. Wang, R. M. Bullock and T. J. Meyer, Energy Environ. Sci., 2016, **9**, 3693–3697.
5 (a) Y. Ooyama, M. Kanda, K. Uenaka and J. Ohshita, ChemPhysChem, 2015, **16**, 3049–3057; (b) E. L. Tae, S. H. Lee, J. K. Lee, S. S. Yoo, E. J. Kang and K. B. Yoon, J. Phys. Chem. B, 2005, **109**, 22513–22522; (c) B.-K. An, W. Hu, P. L. Burn and P. Meredith, J. Phys. Chem. C, 2010, **114**, 17964–17974; (d) Y. Ooyama and Y. Harima, ChemPhysChem, 2012, **13**, 4032–4080.
6 (a) Z. Tachan, I. Hod and A. Zaban, Adv. Energy Mater., 2014, **4**, 1301249; (b) G. Zhang and W. Choi, Chem. Commun., 2012, **48**, 10621–10623; (c) G. Zhang, C. Kim and W. Choi, Catal. Today, 2017, **281**(Part 1), 109–116.
7 P. Persson, R. Bergström and S. Lunell, J. Phys. Chem. B, 2000, **104**, 10348–10351.
8 C. A. Caputo, L. Wang, R. Beranek and E. Reisner, Chem. Sci., 2015, **6**, 5690–5694.
9 M. Bledowski, L. Wang, A. Ramakrishnan and R. Beranek, J. Mater. Res., 2013, **28**, 411–417.
10 (a) Y. Di Iorio, H. B. Rodríguez, E. San Román and M. A. Grela, J. Phys. Chem. C, 2010, **114**, 11515–11521; (b) Q. Li, Y. Che, H. Ji, C. Chen, H. Zhu, W. Ma and J. Zhao, Phys. Chem. Chem. Phys., 2014, **16**, 6550–6554.
11 (a) P. Z. Araujo, P. J. Morando and M. A. Blesa, Langmuir, 2005, **21**, 3470–3474; (b) M. Rodenstein, S. Zürcher, S. G. P. Tosatti and N. D. Spencer, Langmuir, 2010, **26**, 16211–16220.
12 M. A. Gross, A. Reynal, J. R. Durrant and E. Reisner, J. Am. Chem. Soc., 2014, **136**, 356–366.
13 Y. Wang, K. Hang, N. A. Anderson and T. Lian, J. Phys. Chem. B, 2003, **107**, 9434–9440.
14 E. T. Hwang, K. Sheikh, K. L. Orchard, D. Hojo, V. Radu, C.-Y. Lee, E. Ainsworth, C. Lockwood, M. A. Gross, T. Adschiri, E. Reisner, J. N. Butt and L. J. C. Jeuken, Adv. Funct. Mater., 2015, **25**, 2308–2315.
15 (a) G. Li, C. P. Richter, R. L. Milot, L. Cai, C. A. Schmuttenmaer, R. H. Crabtree, G. W. Brudvig and V. S. Batista, Dalton Trans., 2009, 10078–10085; (b) J. T. Carneiro, T. J. Savenije, J. A. Moulijn and G. Mul, J. Phys. Chem. C, 2011, **115**, 2211–2217.
16 D. Mersch, C.-Y. Lee, J. Z. Zhang, K. Brinkert, J. C. Fontecilla-Camps, A. W. Rutherford and E. Reisner, J. Am. Chem. Soc., 2015, **137**, 8541–8549.
17 M. Kato, T. Cardona, A. W. Rutherford and E. Reisner, J. Am. Chem. Soc., 2013, **135**, 10610–10613.
18 D. Hojo, T. Togashi, D. Iwasa, T. Arita, K. Minami, S. Takami and T. Adschiri, Chem. Mater., 2010, **22**, 1862–1869.
19 Y. Zhao, J. R. Swierk, J. D. Megiatto Jr., B. Sherman, W. J. Youngblood, D. Qin, D. M. Lentz, A. L. Moore, T. A. Moore, D. Gust and T. E. Mallouk, Proc. Natl. Acad. Sci. U. S. A., 2012, **109**, 15612–15616.
20 W. Hamd, M. Chavarot-Kerlidou, J. Fize, G. Muller, A. Leyris, M. Matheron, E. Courtin, M. Fontecave, C. Sanchez, V. Artero and C. Laberty-Robert, J. Mater. Chem. A, 2013, **1**, 8217–8225.